Shear-Wave Splitting Observed by Wide-Angle Measurement

Michael Bopp *)

Summary

The recordings of the wide-angle shots by 3-component geophones in the KTB pilot hole exhibit the effect of shear-wave splitting, that is the most diagnostic evidence of seismic anisotropy (Crampin, 1989). The possible reasons for seismic anisotropy will be discussed and the lateral extension of the anisotropic region will be estimated.

Shear-wave observations in the KTB pilot hole

Shear-wave splitting has been observed for Vogtland earthquakes, recorded at seismological stations NE of the KTB location (Schmedes, 1987). By recording the wide-angle shots of the ISO89

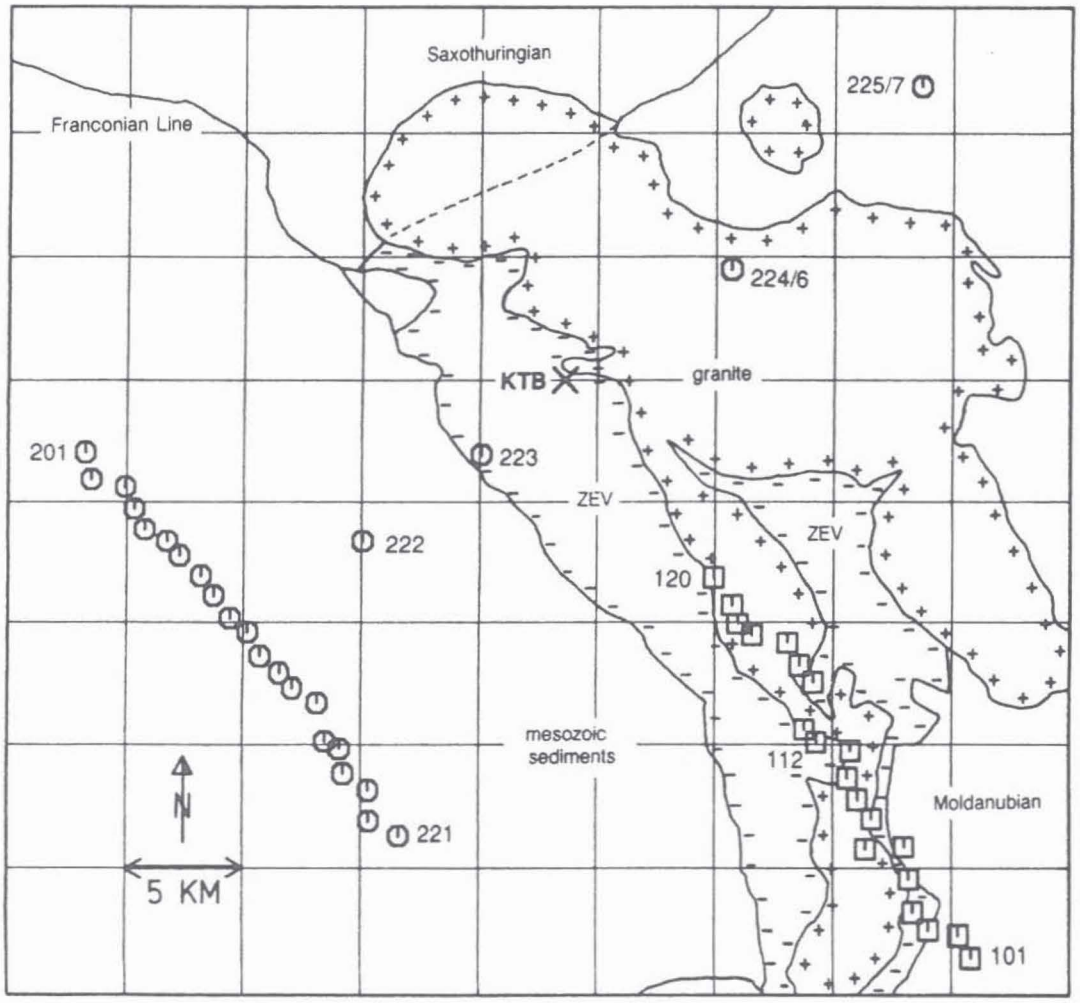

Fig. 1: Location map of ISO89 wide-angle measurement superimposed with a simplified geology (after Stettner, 1981) of the KTB surrounding. ZEV is the Zone of Erbendorf Vohenstrauß; numbers indicate shots.

*) Institut f. Allg. u. Angew. Geophysik, Theresienstr. 41/IV, D-8000 München 2, FRG

survey (**Fig. 1**; Gebrande et al., 1990) with 3-component geophones in the KTB pilot hole an independent check of the splitting effect became possible. Borehole recordings have the special advantage of being free from the usual distortions by the earth's surface, e.g. non-orthogonality of P- and S-polarization directions and non-linearity of S-polarization.

Decomposition of the 3-component recordings into mutually orthogonal components parallel and normal to P-wave polarization provides an almost perfect separation of P- and S-waves. **Fig. 2** shows the seismogram section for the shotpoints 101-120 in the SE of the KTB location, recorded in 3270 m depth. The traveltime, √3-times greater than for P-waves, and the lower frequency content of the shear-waves indicate primary radiation from the source and no P-S conversions. Most likely, anisotropy and local heterogeneities of the crystalline source environment are responsible for the S-wave radiation. The shear-wave is not of pure SV- or SH-type, since it can be seen on the vertical and transverse horizontal component in Fig. 2. Its polarization is in the plane normal to P-wave polarization, proving shear-wave propagation parallel to the P-wave.

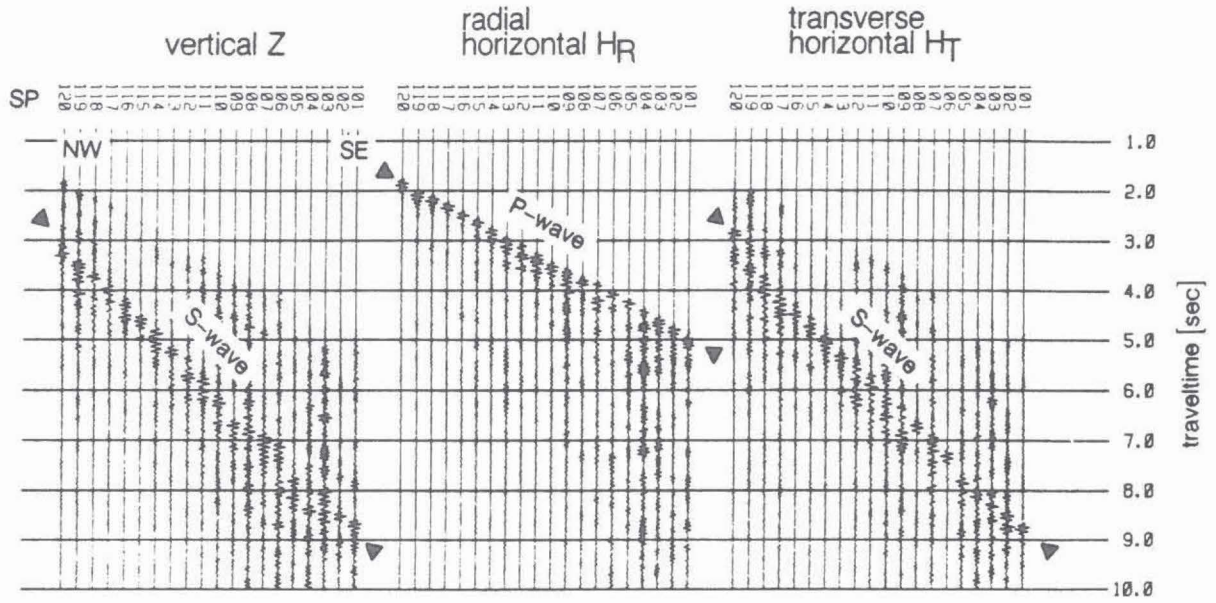

Fig. 2: Seismogram sections of SPs 101-120 for the 3-component receiver in 3270 m depth. A 6-15 Hz band-pass filter was applied to improve the appearence of shear-waves. Each trace is normalized to its maximum amplitude.

The recordings of SP 113 (**Fig. 3a**) show two shear-wave onsets with a time delay of nearly 0.2 s. The fast quasi shear-wave **qS1** (terminology after Crampin, 1989) with linear polarization dipping steeply to SW is followed by the slow quasi shear-wave **qS2** with more elliptical horizontal polarization. These properties can be seen from the polarization diagrams (**PD**) in the plane normal to P-wave polarization (**Fig. 3b**). It's a characteristic effect of S-wave propagation through an anisotropic medium. The fast qS1-wave is expected to be polarized in a preferred direction of anisotropy and the slow qS2-wave is perpendicular to this. A strict orthogonality is, however, not observed in the real data and possible reasons will be discussed later.

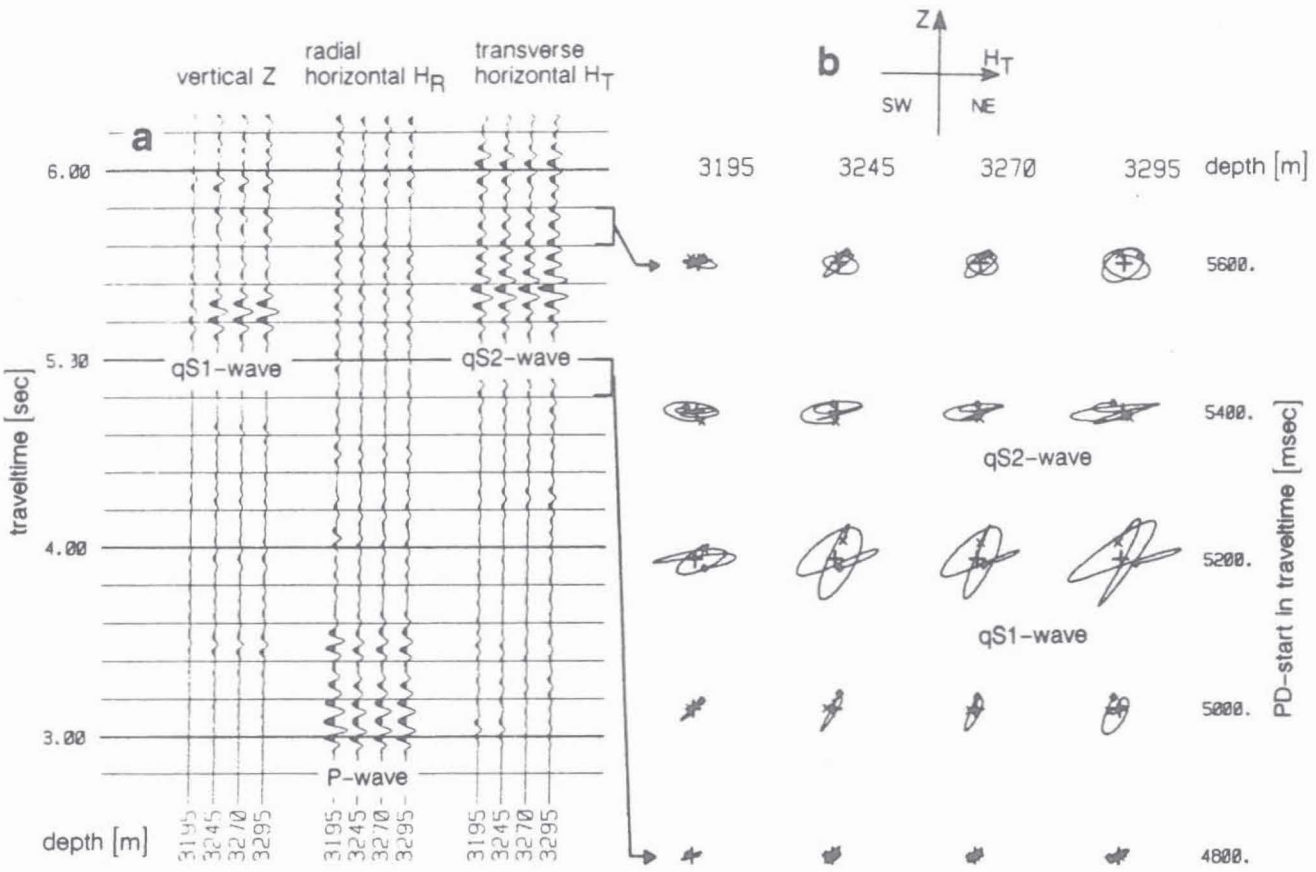

Fig. 3: Unscaled seismogramms (**a**) and polarization diagrams (PD, **b**) in the plane normal to P-wave polarization showing shear-wave splitting for SP 113. All PDs are plotted with the same gain.

Causes for seismic anisotropy

Seismic anisotropy in the continental crust is mainly due to the following reasons (Crampin et al., 1984):

a) Parallel (micro-)cracks, occasionally filled with fluids (**E**xtensive **D**ilatancy **A**nisotropy).

b) Interbedding of rocks (foliation) that can be isotropic itself (**P**eriodic **T**hin-**L**ayer Anisotropy).

After Crampin (1989) EDA-anisotropy caused by vertically aligned cracks, that are generally orientated normal to the minimum compressive stress, should be wide-spread over the crust. Field observations have been interpreted in either way. Ahmed (1990) estimated the axis of maximum horizontal compressive stress from splitted shear-waves observed in a VSP-survey by identifying the polarization of the fast qS1-wave with the orientation of open micro-cracks (case **a**). On the other hand Brocher and Christensen (1990) observed maximum P-wave velocity in a seismic survey in the direction perpendicular to the axis of maximum compressive stress, but parallel to rock foliation, and explained this result by PTL-anisotropy and mineral orientation (case **b**).
Comparison with laboratory investigations on KTB cores should elucidate, whether case **a** and/or **b** is responsible for the observed shear-wave splitting in Fig. 3b.

Significant velocity anisotropy is present in most KTB core samples (Lippmann et al., 1989; Zang et al., 1989; Kern et al.,

1991). Their maximum P-wave velocity is generally observed parallel to foliation in gneisses. A larger part of this anisotropy is caused by micro-cracks aligned parallel to the foliation, because it diminishes with increasing pressure (case **a**; Zang et al., 1989, Kern et al., 1991). The remaining intrinsic anisotropy of about 10% in gneisses is a textural one (case **b**) and is caused by preferred orientation of anisotropic minerals as, e.g., micas in gneisses and hornblende in amphibolites (Kern et al., 1991). Crack and textural anisotropy interfere constructively, because the orientation of the cracks is coupled to the foliation. At in-situ conditions the textural cause is expected to dominate.

Ultrasonic measurements of shear-wave splitting in core samples (Kern et al., 1991) are even more important for the interpretation of the field data. In gneisses it is most pronounced for S-wave propagation parallel to the foliation with the fast qS1- and the slow qS2-wave being polarized parallel and normal to the foliation plane. Velocity differences up to 15% due to shear-wave splitting are expected at in situ pressures in gneisses.

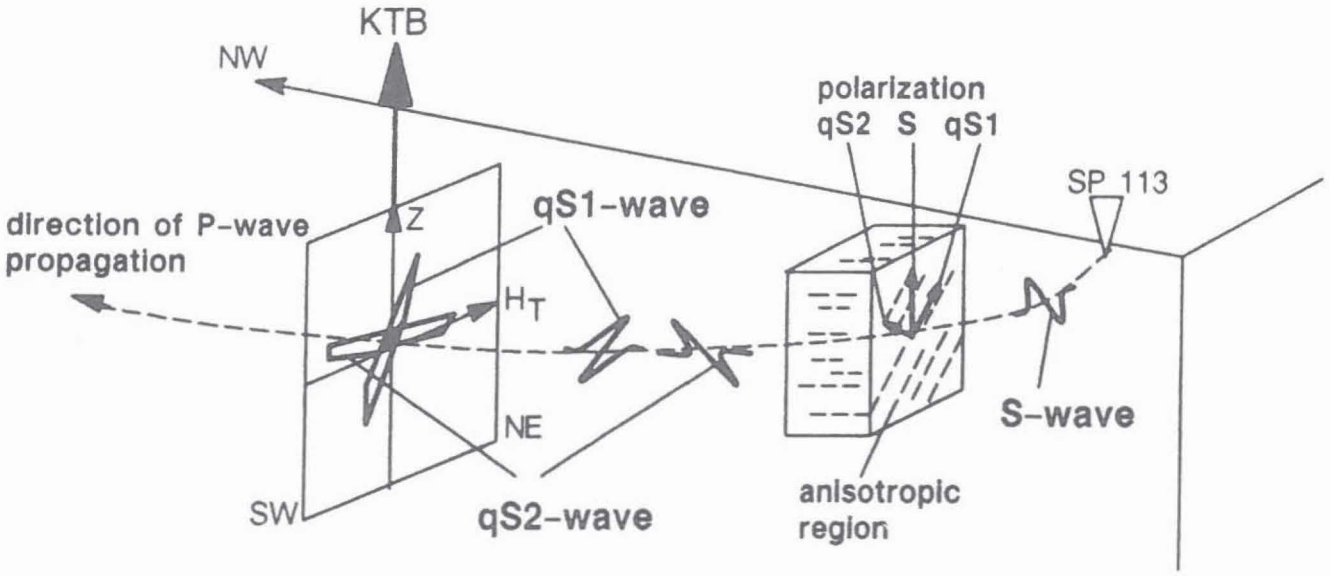

Fig. 4: Schematic illustration (modified after Crampin, 1989) that combines the observed shear-wave splitting with the results from ultrasonic measurements. A primary generated S-wave propagates through a region with foliation dipping steeply to SW and splits up into a fast qS1- and a slow qS2-wave.

In **Fig. 4** the simplified observation from the PDs in Fig 3b is combined with the results from laboratory investigations. The shear-wave generated e.g. by SP 113 propagates through a region with foliation dipping steeply to SW. The shear-wave splitting must be related to both effects, **a** (micro-cracks), and **b**

---

on right page:

Fig. 5: Results of polarization analyses of the 4 down-hole 3-component recordings (**a** to **d**) of SP 113. For each receiver position 3 plots are presented: 3-component seismograms on the lower right side, polarization parameters to the left as a Schmidt diagram and on the upper right side as functions of time. The P-wave polarization is almost horizontal and close to the shot-to-receiver azimuth. The shear-wave splitting is most pronounced for geophones at 3245 m (**b**), 3270 m (**c**) and 3295 m depth (**d**) with steep dipping qS1-polarization and almost horizontal qS2-polarization under the same azimuth.

POLARIZATION VECTOR
FOR SHOT 113 AND DEPTH 3195
↑ SHOT TO RECEIVER AZIMUTH 325.0 [DEG]

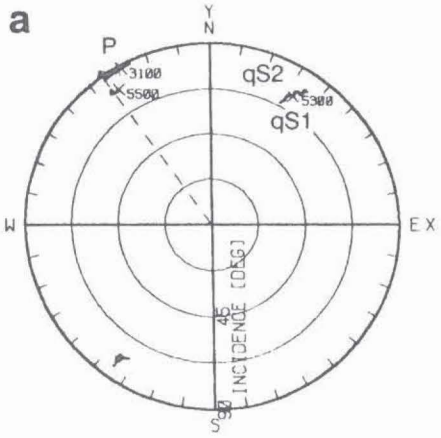

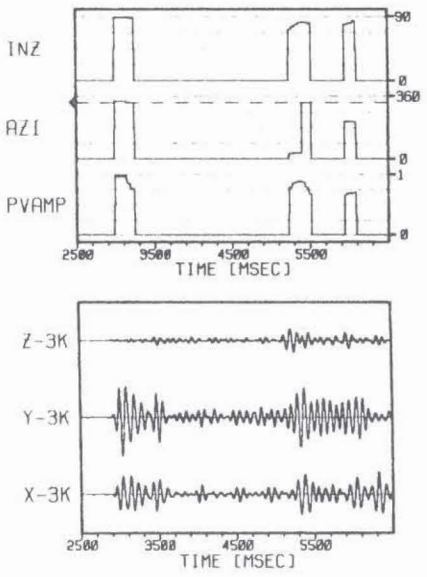

POLARIZATION VECTOR
FOR SHOT 113 AND DEPTH 3245
↑ SHOT TO RECEIVER AZIMUTH 325.0 [DEG]

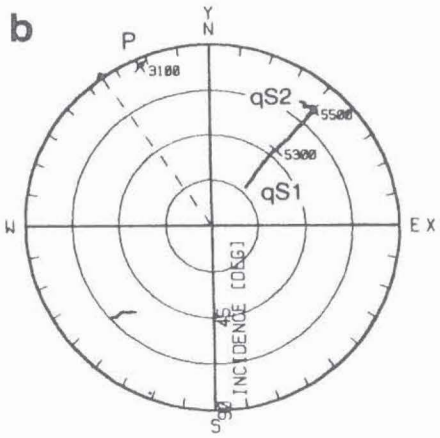

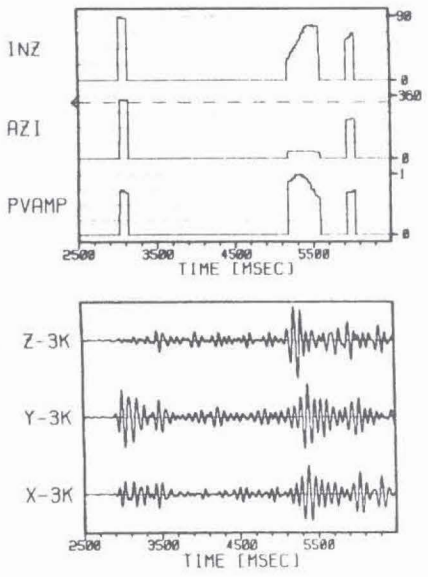

POLARIZATION VECTOR
FOR SHOT 113 AND DEPTH 3270
↑ SHOT TO RECEIVER AZIMUTH 325.0 [DEG]

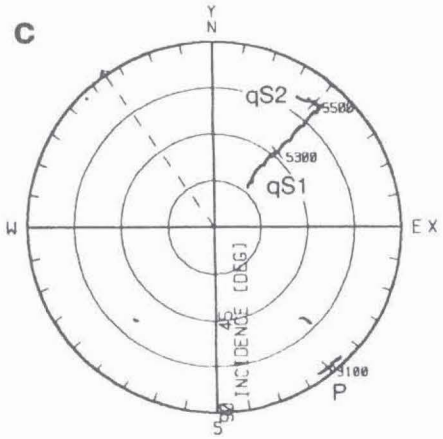

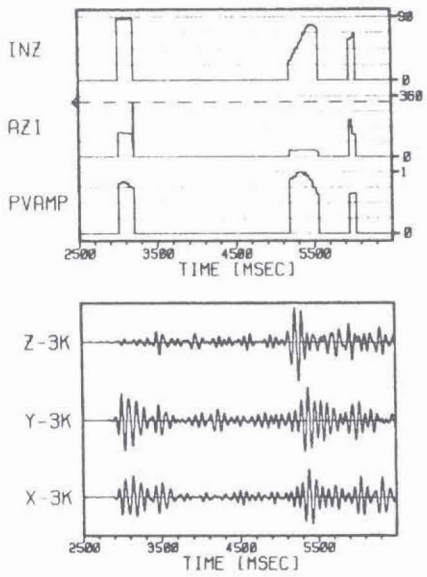

POLARIZATION VECTOR
FOR SHOT 113 AND DEPTH 3295
↑ SHOT TO RECEIVER AZIMUTH 325.0 [DEG]

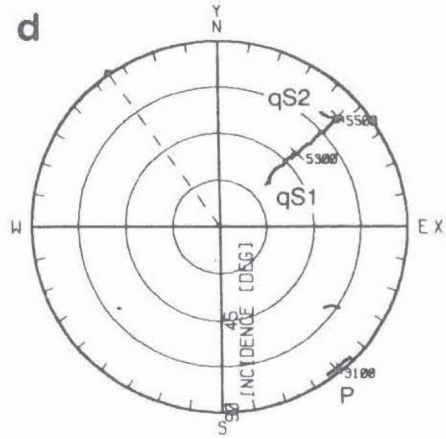

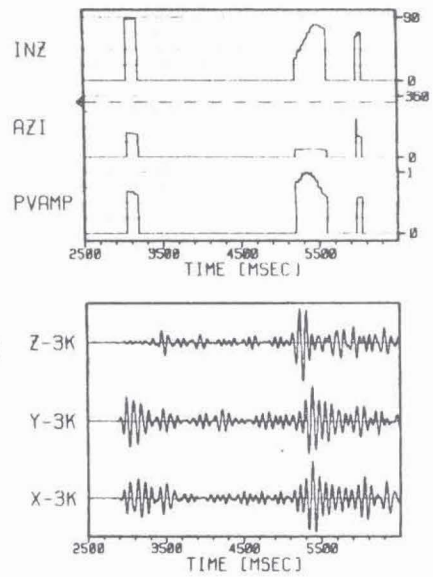

(texture). Cracks are not necessarily closed in the depth range of wave propagation as indicated by an open joint found at 3447 m depth (Stroh et al., 1990).

According to this model the dip of foliation can be obtained by the polarization of the fast qS1-wave (Crampin, 1985) assuming homogeneous anisotropy and wave propagation parallel to the strike of foliation. **Figs. 5a-d** show the results of polarization analysis for SP 113 using the so-called polarization vector (Bopp, 1992). The polarization parameters, azimuth (**AZI**) and angle of incidence (**INZ**), measured from the vertical, are calculated in sliding time windows of 200 ms. They are plotted as time dependent traces in a Schmidt diagram (left side in Figs. 5a-d). The "trace" of the polarization vector amplitude (**PVAMP**) is plotted together with the polarization parameters as function of time (upper right side). The magnitude of PVAMP is used to define a valid polarization result (s. chapter 3.2 in Bopp, 1992).

The P-wave (at 3100 ms) is almost horizontally polarized (INZ≈90°) close to the shot-to-receiver azimuth at all geophone depths (Figs. 5a-d). The estimated azimuth may be in the opposite direction (s. Fig. 5c and 5d) for inclined polarization, because it changes by 180° when the inclination crosses the horizontal plane (INZ≡90°).

At the deeper-located geophones (Figs. 5b-d) the angle from vertical to the qS1-polarization (before 5300 ms) amounts to ≈30° whereas the qS1-polarization at 3195 m depth (Fig. 5a) shows small dip (INZ≈70°). While instrumental effects should be excluded this observation fits to almost horizontal foliation at 3100 m depth and a fault zone at 3200 m depth (Röhr et al., 1990).

The qS2-polarization is almost horizontally polarized (INZ≈80°) at all depths. Because the azimuthal direction (≈40 N°E) is the same for qS1- and qS2-polarization, it can be assumed that the splitted shear-waves are propagating in the same direction.
From the qS1-polarization in 3245-3295 m depth it appears that the dip of foliation SE of the KTB location is about 60° to SW.

Lateral extension of the anisotropic region SE of KTB

Fig. 6 shows the PDs recorded in 3245 m depth for all SP 101-120 SE of the KTB location. The plane of the PDs normal to P-wave polarization is individually adjusted for each shot. The amplitudes in the vertically arranged PDs are scaled to the maximum trace amplitude within this shot.

SP 113 exhibits the most pronounced shear-wave splitting. It is less distinct for the adjacent SP 111-116. The observed S-wave from SP 106 seems to be of pure SH-type. In general only the SP 112-120 nearest the KTB location exhibit the steep dipping qS1-polarization. Averaging these dip angles, measured from the horizontal and calculated with a polarization analysis by solving the 2D-covariance matrix for eigenvalues and -vectors (Kanasewich, 1973), leads to the results demonstrated in **Tab. 1.**

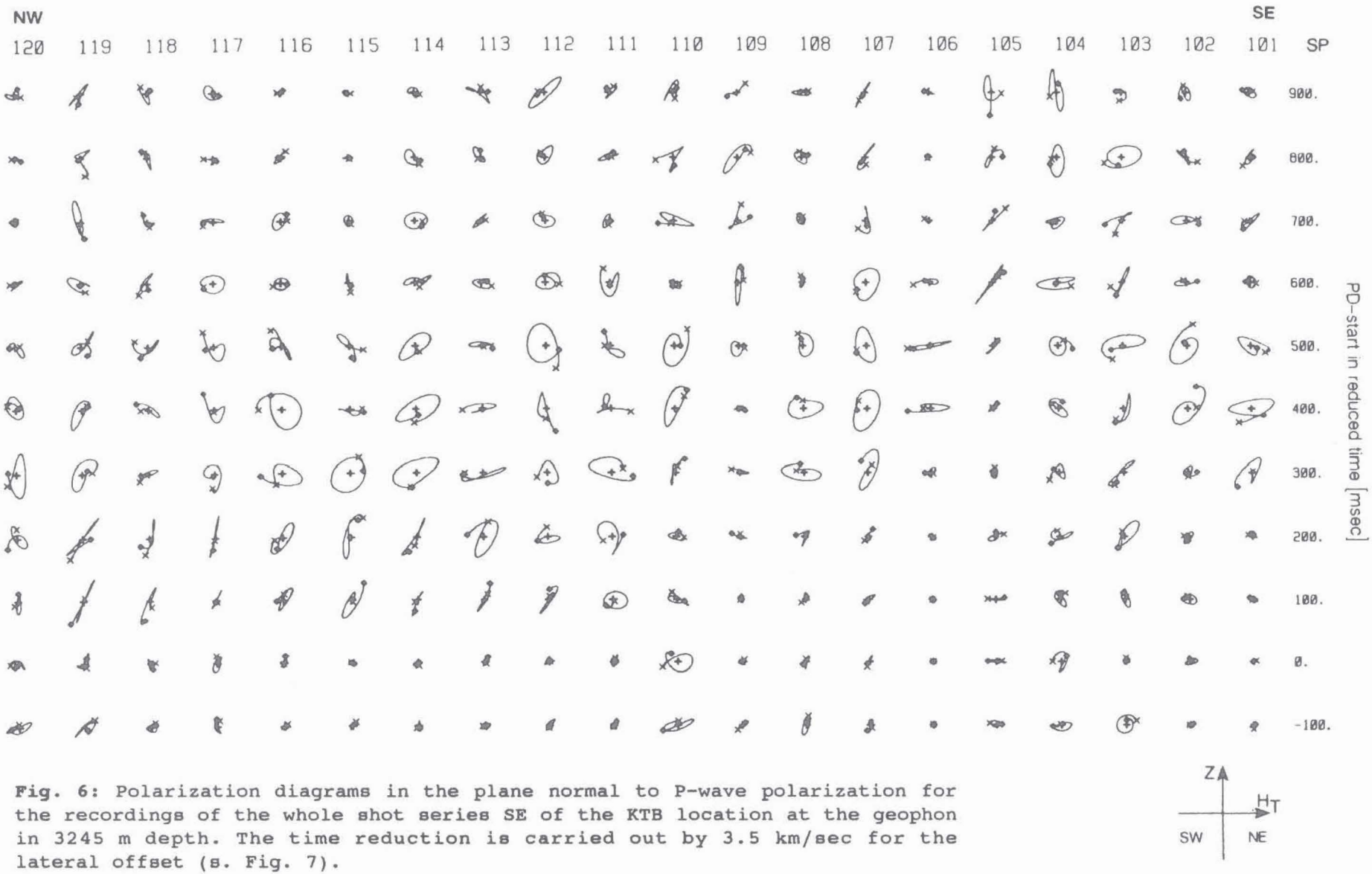

Fig. 6: Polarization diagrams in the plane normal to P-wave polarization for the recordings of the whole shot series SE of the KTB location at the geophon in 3245 m depth. The time reduction is carried out by 3.5 km/sec for the lateral offset (s. Fig. 7).

Table 1: Comparison between the qS1-polarization obtained by averaging the results of polarization analysis for SPs 112-120 and the dip of rock foliation determined at KTB core samples. Dip angles are measured from the horizontal.

geophone depth [m]	3195	3245	3270	3295
Dip of polarization to SW [°] (mean value with standard deviation)	37 ± 13	68 ± 10	68 ± 10	65 ± 10
Dip of foliation in the borehole [°]	35	30	35	40

The difference in the polarization angles between the uppermost and the deeper-seated geophones is about 30°. These polarization dips are compared in Tab. 1 with the dip of rock foliation (moving average over 25 m; from Fig. 4 in Lippmann et al., 1989). In the depth interval of the geophones (**Fig. 7a**) azimuth and dip of rock foliation are not uniform (Kohl et al., 1991). This implies that the immediate surrounding of the down-hole geophones can't be responsible for the observed shear-wave splitting with qS1-polarization dipping to SW.

The VSP-surveys of ISO89 provided complementary observations of shear-wave splitting for vertical wave propagation (Lüschen et al., 1990) with the fast qS1-wave being polarized NW-SE. According to the authors this may be due to the uniform NW-SE striking and steeply SW-dipping foliation in the depth range 1500 to 2700 m (**Fig. 7b**). If this zone extends further to the SE, it could consistently also explain the wide-angle observations, since the ray-paths for the wide-angle shots, calculated by raytracing (Gebrande et al., 1990), are nearly horizontal in this depth range.

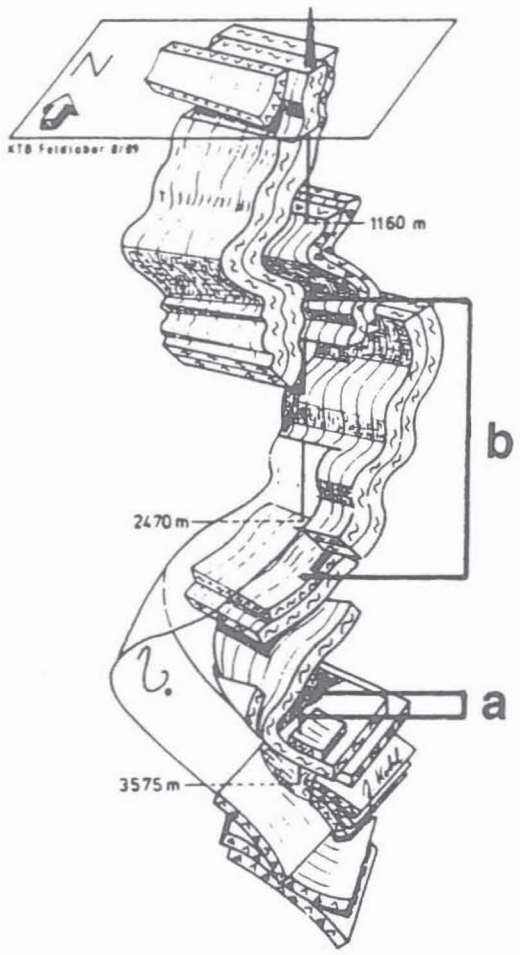

Fig. 7: Schematic sketch of the geological section in the KTB pilot hole (Röhr et al., 1990) marked in the depth ranges of: geophone locations (**a**); uniform dipping foliation, mentioned in the text (**b**).

Fig. 8 shows record sections of the decomposed fast qS1- and slow qS2-wave for the total shot series recorded at 3245 m depth. As well as in Fig. 6 the shear-wave splitting is most evident for SPs 111-119. Surprisingly, the time difference between the qS1- and qS2-waves, marked by arrows (▸) in Fig. 8a and 8b, does not increase with distance but remains constant about 0.2 s. This indicates that the anisotropy producing the splitting effect cannot be homogeneous between the borehole and the shotpoints. Homogeneity seems to be confined to a common segment of the

raypaths somewhere between the KTB location and shotpoint 120. From the geology (Fig. 1) this is, indeed, not surprising, since the shotpoints 112 to 120 are situated in probably isotropic granites, but the complementary wave paths cross foliated metamorphic rocks of the ZEV (**Z**one of **E**rbendorf-**V**ohenstrauß).

Assuming a splitting coefficient $A=(V_{qS1}-V_{qS2})/V_{qS1}$ of 10% (Kern et al., 1991) and a velocity of 3.5 km/s for the qS1-wave, the diameter **L** of the anisotropic source area can be estimated from the observed qS2 to qS1 delay time dT (0.2 s from Fig. 8) by the equation: $L = (V_{qS2} \cdot dT) / A$
giving **L = 6.3 km/s**. This is less than the distance from SP 120 to the borehole.

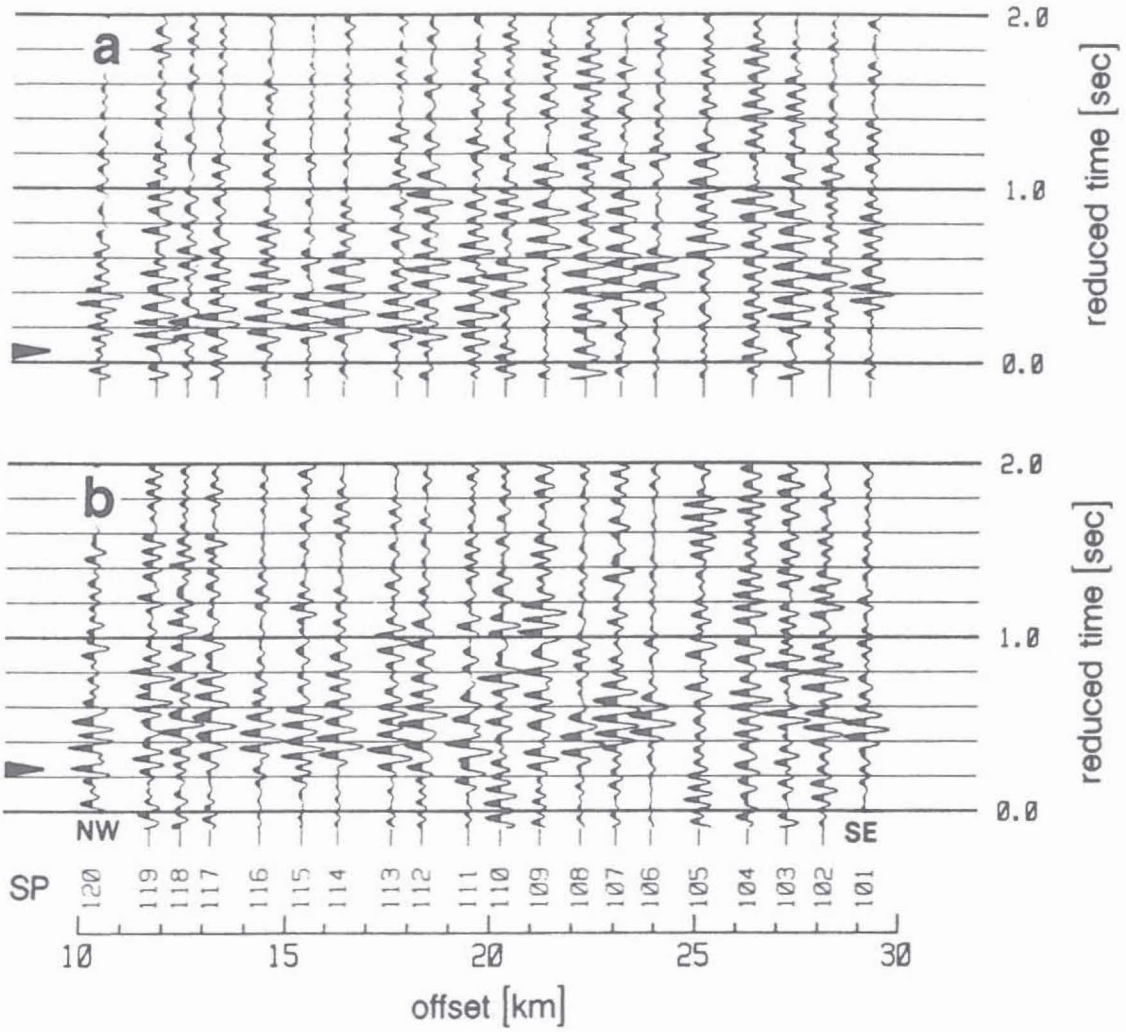

Fig. 8: Comparison of the separated fast qS1- (**a**) and slow qS2-wave (**b**) for all shotpoints recorded at 3245 m depth. The trace-normalized seismograms are plotted versus the lateral offset reduced by 3.5 km/s. The time delay between the onsets marked by (▸) of the fast qS1- and slow qS2-wave is almost 0.2 s.

Discussion

The question arises, why shear-wave splitting is not observed for the more distant shotpoints 101 to 110 (Fig. 6) in spite of at least partially the same raypaths. Several reasons may be responsible for this. First of all the polarization direction of

the primary generated S-wave is accidental in contrast to the Vibroseis VSP-survey mentioned above, because the shooting technique has not been designed for S-wave radiation. Both polarization directions, qS1 and qS2, must be excited to observe shear-wave splitting. SP 106 in Fig. 6 may represent this case, where only one polarization direction is stimulated, because the primary S-wave polarization is parallel or normal to the foliaton.

An extreme case for accidental or absent S-wave radiation is shown in **Fig. 9** for the shotpoints situated in the sediments SW of KTB (s. Fig. 1). In spite of the same shooting technique and preprocessing parameters there are no significant onsets beside the direct P-wave compared with Fig. 2 and it seems that no shear-waves have been radiated. Shear-wave generation is related to heterogeneities in the immediate source surrounding and fractures that contribute to this heterogeneity in crystalline rocks are absent in sedimentary rocks.

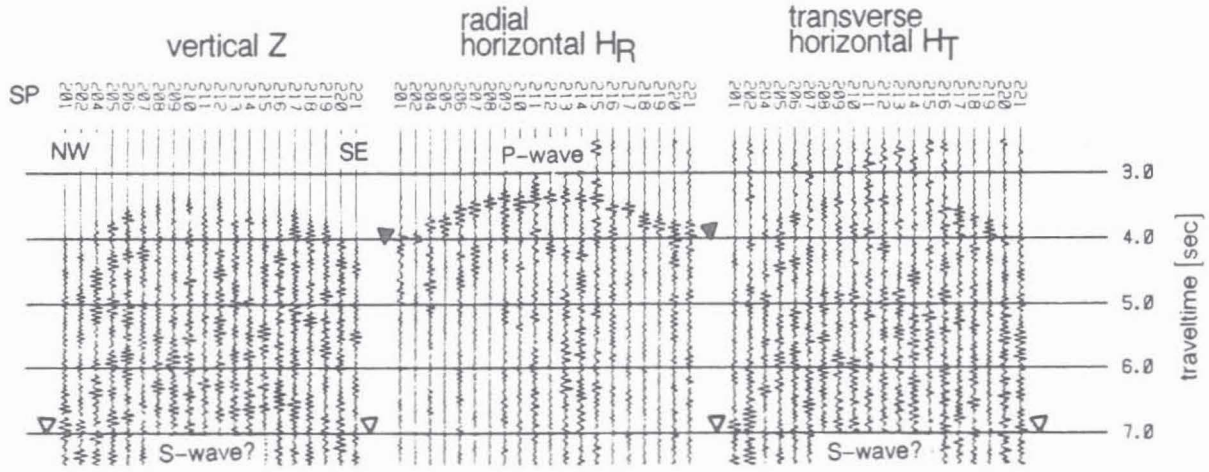

Fig. 9: Seismogram sections of SPs 201-221 for the 3-component receiver in 3220 m depth. The 6-15 Hz band-pass filtered seismograms are normalized to maximum amplitude within each trace. There are no significant S-wave onsets at this traveltime (open triangles) where they should appear for a V_P/V_S-ratio of $\sqrt{3}$ (s. Fig. 2).

Other reasons for the extinction of splitting effects can be due to reflection and refraction. As an extreme case suppose a splitted shear-wave with orthogonally polarized components hits an interface at the Brewster angle of SH-waves. Then only the SV-components of the qS1- and qS2-waves are reflected and both waves will have the same polarization.

Finally the effect of heterogeneous anisotropy should be considered. For simplicity a sequence of homogeneous anisotropic layers as in Fig. 4 with constant strike but different dip angles of foliation is assumed. The qS1- and qS2-wave generated in the first medium will be generally split further. This results in a stretched shear-wavetrain and it is uncertain whether single shear-wavelets can be separated. Because the amplitude of the leading qS1-wave is generally diminished during each change in foliation and its time lead may presumable be less than the duration of the primary source generated S-wavelet, it becomes succesively more unlikely that it can be resolved at all.

Conclusions

Summarizing the results of wide-angle recordings in the KTB pilot hole it can be stated:

- Seismic anisotropy in the crystalline KTB surrounding is proved by the observed shear-wave splitting.
- From comparison with laboratory investigations rock foliation is expected to be the main cause of anisotropy.
- The observed qS1-polarization and the time difference between the split shear-waves can be explained in the simplest way by assuming foliated rocks with an average foliation dip of 60-70° and a NW-SE extension of ≈6 km at about 3 km depth in the ZEV south-east of KTB.

References

Ahmed, H., 1990. Investigation of azimuthal anisotropy from offset VSP data - a case study, First Break, **8**, 449-457.

Bopp, M., 1992. Kombinierte Polarisations- und Arrayanalyse seismischer Daten im KTB-Umfeld, Diss. Ludwig-Maximilians-Universität München, in preparation.

Brocher, T.M., Christensen, N.I., 1990. Seismic anisotropy due to preferred mineral orientation observed in shallow crustal rocks in southern Alaska, Geology, **18**, 737-740.

Crampin, S., 1985. Evaluation of anisotropy by shear-wave splitting, Geophysics, **50**, 142-152.

Crampin, S.,1989. Suggestions for a consistent terminology for seismic anisotropy, Geophysical Prospecting, **37**, 753-770.

Crampin, S., Chesnokov, E.M., Hipkin, R.G., 1984. Seismic anisotropy - the state of the art: II, Geophys. J. R. astr. Soc., **76**, 1-16.

Gebrande, H., Bopp, M., Meichelböck, M. and Neurieder, P., 1990. 3-D Wide-Angle Investigations in the KTB Surroundings as part of the "Integrated Seismics Oberpfalz 1989 (ISO89)", KTB-Report **90-6b**, NLfB Hannover, 183-208.

Kanasewich, E.R., 1973. Time Sequence Analysis in Geophysics, The University of Alberta press, pp. 352.

Kern, H., Schmidt, R. and Popp, T., 1991. The velocity and density structure of the 4000m crustal segment at the KTB drilling site and their relationship to lithological and microstructural characteristics of the rocks: an experimental approach, Scientific Drilling, **2**, 130-145.

Kohl, J., Kück, J., Sigmund, J., Wöhrl, Th., 1991. Bohrkernorientierung und Teufenkorrelation der KTB Vorbohrung, KTB-Report **91-3**, , NLfB Hannover, F1-F22.

Lippmann, E., Bücker, Ch., Huenges, E., Rauen, A., Wienand, J., Wolter, K. and Soffel, H.C., 1989. Rock physical properties: first results of the KTB-field-laboratory, Scientific Drilling, **1**, 143-149.

Lüschen, E., Söllner, W., Hohrath, A. and Rabbel, W., 1990. Integrated P- and S-Wave Borehole Experiments at the KTB-Deep Drilling Site, KTB-Report **90-6b**, NLfB Hannover, 85-136.

Röhr, C., Kohl, J., Hacker, W., Keyssner, S., Müller, H., Sigmund, J., Stroh, A., Zulauf, G., 1990. German Continental Deep Drilling Program (KTB) - Geological survey of the pilot hole "KTB Oberpfalz VB", KTB-Report **90-8**, NLfB Hannover, B1-B55.

Schmedes, E., 1987. Some results from digital recording with 4 nearby stations, in: Earthquake swarm 1985/86 in Western Bohemia - Proc. of workshop in Mariánské Láznè, December 1986, D. Procházková (ed.), Praha, 124-129.

Stettner, G., 1981. Geologische Karte 1:200000 C 6334 Bayreuth, BGR Hannover.

Stroh, A., Hansmann, J., Heinschild, H.-J., Homann, K.D., Tapfer, M., Wittenbecher, M., Zimmer, M., 1990. Drill Hole KTB Oberpfalz VB, Geoscientific Investigations in the KTB-Field-Laboratory, Depth interval 0 - 4000.1 m, KTB-Report **90-8**, NLfB Hannover, C1-C37.

Zang, A., Wolter, K. and Berckhemer, H., 1989. Strain recovery, microcracks and elastic anisotropy of drill cores from KTB deep well, Scientific Drilling, **1**, 115-126.